Characterization of uranium oxide powders and sinterability

Joakim Ceder

Abstract

Uranium oxide (UO_x) is an energy dense material commonly used in nuclear fuel. UO_x powder is pressed and sintered to produce uranium dioxide (UO_2) pellets which are loaded into fuel rods. The rods are then mounted together in a final nuclear fuel assembly. Stability and predictability of the manufacturing processes during UO_2 pellet production is of high importance. To achieve desired properties and quality of the UO_2 pellets, the ability to assess the characteristics of the UO_x powder is crucial. Sinterability is the most important characteristic which describes the behavior of the UO_x powder during reduction in high temperatures. Recycled uranium dioxide is oxidized into U_3O_8 powder which can be used to modify the sinterability due to its pore forming ability.

This study describes the characterization of uranium oxide powders and pellets regarding physicochemical properties relating to sintering behavior. Statistical analyses of historical data were also performed and showed a complexity of the relation between powder properties and sinterability. The effect of U_3O_8 powder in different blends of UO_2 powders of high and low sinterability were analyzed. Varying U_3O_8 powder batch did not influence the diameter shrinkage after sintering except for one case. UO_2 powder blends showed deviating behavior from their virgin powder constituents.

Chemical activity of UO_2 was analyzed by oxidation with H_2O_2. The consumption rate of H_2O_2 was shown to depend on specific surface area, although further studies are planned.

Index

1 Introduction

Nuclear energy is an important factor in clean energy production for the future. Nuclear fuel is the fuel type with the highest energy to weight ratio available (3.5% enriched uranium has a heat value of 3 900 MJ/kg) [1]. According to the Intergovernmental Panel on Climate Change (IPCC), nuclear power is among the electricity generating sources with the lowest greenhouse gas emissions (12 g CO_2eq/kWh) [2]. In 2017 the combined 446 nuclear reactors worldwide produced 2 561 TWh of electricity meaning about 10.3% of worldwide electricity production. In Sweden, for the same period, 8 reactors produced 63.8 TWh which corresponds to 40.3% of the country's total electricity production [3]. Westinghouse Electric Sweden AB manufactures nuclear fuel in its Västerås facilities, where it has been produced since the 1960's.

1.1 Nuclear power production

A nuclear power reactor could be described as a large water boiler. The nuclear reactions taking place inside the core – the splitting of the uranium atom – release large amounts of energy that converts water into steam. There are several different types of nuclear reactors in operation around the world; three common ones are the Boiling Water Reactor (BWR), Pressurized Water Reactor (PWR) and Water-Water Energetic Reactor (VVER). In a BWR, the steam generated in the reactor vessel directly drives a turbine for electricity generation, see Figure 1. In a PWR the primary hot water heat exchanges with a steam generator and the steam in the secondary circuit drives the turbine, see Figure 2. The VVER was developed in the Soviet Union and is a type of Pressurized Water Reactor. The reactor power output is varied by withdrawing or inserting control rods into the core. A neutron absorbing material in the control rods absorbs the neutrons that would otherwise perpetuate the nuclear reactions.

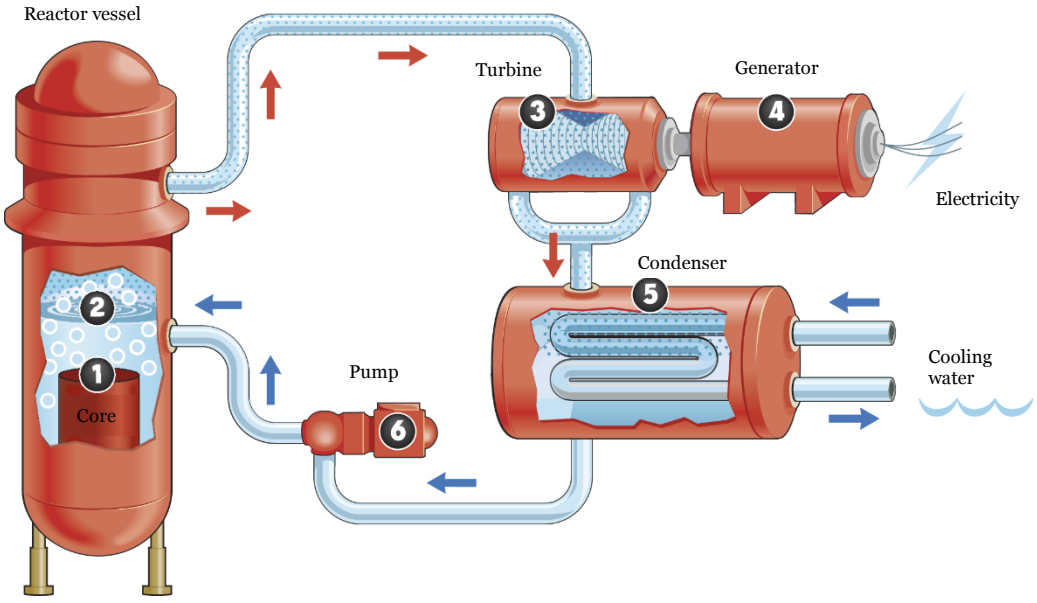

Figure 1. Schematic image of a Boiling Water Reactor [4].

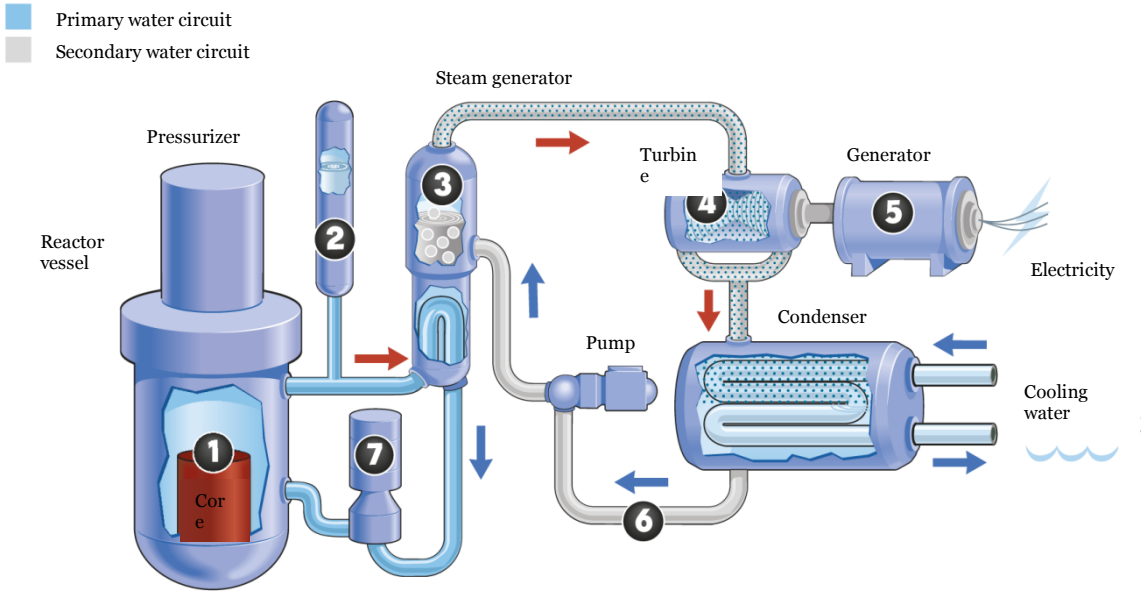

Figure 2. Schematic image of a Pressurized Water Reactor [4].

The different nuclear reactor designs use different nuclear fuel assembly designs. BWR fuel assemblies consist of up to 11x11 fuel rods covered by a box. The fuel assembly is in contact with both liquid water and steam. PWR fuel assemblies are only in contact with liquid water and are not covered by a box. They consist of up to 18x18 fuel rods. VVER fuel assemblies are hexagonally shaped, see Figure 3.

The fuel tubes are typically up to 4 m long and made from different zirconium alloys. A fuel rod is a fuel tube which has been loaded with cylindrically shaped ceramic UO_2 pellets, about 7–10 mm in diameter and 9–11 mm in height. A description of the nuclear fuel manufacturing process follows.

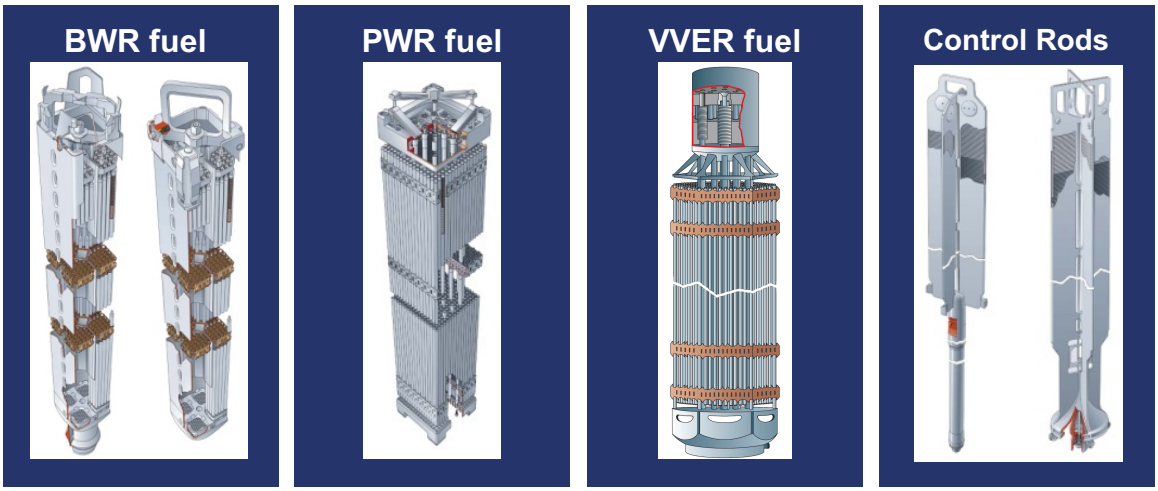

Figure 3. Nuclear fuel designs and components [5].

1.2 The nuclear fuel manufacturing process

The process starts with the conversion of uranium oxide powder (UO_x). The UO_x powder is pressed and sintered into pellets, which are loaded into fuel rods, packaged into fuel bundles and mounted as fuel assemblies, see Figure 4. The fuel assemblies are delivered to nuclear power plants all around the world.

Figure 4. The nuclear fuel manufacturing process – from UF_6 cylinders, to pelletizing, to loading and shipping [5].

UO_x powder can be converted from two different source materials, Uranium Nitrate Hexahydrate (UNH – $UO_2(NO_3)_2 \cdot 6\ H_2O$) or Uranium Hexafluoride (UF_6). UNH originates from the dissolution of recycled uranium in nitric acid. UF_6 is the most commonly used starting material and it can be converted into UO_2 through several routes. One route is to convert UF_6 into UO_2 via Ammonium Uranyl Carbonate (AUC – $(NH_4)_4UO_2(CO_3)_3$).

UF_6 (s) is vaporized and reacts in water with ammonium and carbonate ions to precipitate Ammonium Uranyl Carbonate particles. The temperature of the precipitation, as well as the concentrations of the added chemicals, determine the final UO_2 particle size, as it follows the grain size of the AUC precipitate [6]. The chemical formula of the AUC process of conversion from UF_6 into UO_2 via Ammonium Uranyl Carbonate is as follows:

$$UF_6 + 4\ NH_4OH + 3\ (NH_4)_2CO_3 \rightarrow (NH_4)_4UO_2(CO_3)_3 + 6\ NH_4F \qquad \text{[Eq 1]}$$

The precipitate is washed and dried on a rotary filter and thereafter reduced to UO_2 during hydropyrolysis. In the final step the UO_2 powder is exposed to air to create a thin layer of stable U_3O_8 on the UO_2 particle surfaces. The particle size that was set in the precipitation step is influencing the behavior of the powder in the fluidized bed furnace. The degree of fluidization and the effective heat transfer inside the furnace determine other powder properties such as specific surface area, crystallinity, grain size, bulk density and stoichiometry [7]. An advantage of the AUC process is the free-flowing powder it produces which can be handled without further processing steps or additives.

The powder is pressed into so called green pellets. To reach the target pellet dimensions, density, diameter and height, the powder is pressed at a certain pressure in a die of suitable size. Higher pressure gives higher green density. The green pellets are sintered in a reducing atmosphere composed of hydrogen (H_2) and carbon dioxide (CO_2). The CO_2 addition is minor compared to the hydrogen and its purpose is to control the oxygen content. During sintering the particles are rearranged to create a closely packed system to minimize the free energy in the pellet. This leads to densification and the pellet effectively shrinks approximately 50% in volume and 15–20% in diameter. The definition of sintering is to form a solid mass by heat or pressure without melting the material. The sintering process consists of several steps with different temperatures and gas compositions. In the beginning of the process the temperature is high enough to drive off impurities while later it is increased to above 1700°C . The reduction from UO_x to UO_2 and the rearrangement of particles occurs during the final steps at the highest temperatures. Important parameters for controlling the sintered pellet properties are gas composition and flow, temperature profile and UO_x powder properties.

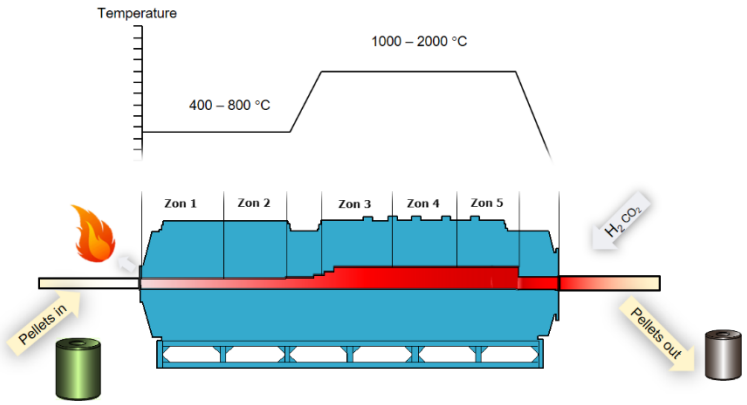

Figure 5. Schematic image of a sintering furnace.

The sintered pellets are ground to a target diameter depending on design of the final nuclear fuel assembly. To minimize the amount of recycled material and to maximize process efficiency a grinding margin of ≥0.05 mm is desired. Pellets which do not meet the criteria for diameter and/or other visual defects are rejected and recycled, see Figure 6.

Figure 6. An example of the visual inspection of sintered UO_2 pellets [5].

1.3 Oxidized material U_3O_8

Recycled material, such as rejected pellets or grinding waste, are oxidized to U_3O_8 powder and recovered back into the pellet manufacturing process by blending with UO_2 powder. The recycled material is heat treated at around 450°C during approximately 4 hours with addition of air and is later homogenized before being added into the UO_2 powder.

In the process of oxidizing the recycled material into U_3O_8, the stress build-up breaks the material down into a powder with small, sharp and cracked particles [8], see Figure 19. The size range of the U_3O_8 particles is around 10 µm [9]. The morphology of the U_3O_8 powder particles allows them to wedge in between the larger UO_2 particles. When the U_3O_8 particles are reduced to UO_2 in the sintering furnace they shrink, and channels are formed from where trapped impurities can escape. After completion of the sintering process the channels have transformed into pores at the contact points with adjacent UO_2 particles. For this reason, U_3O_8 powder is called a “pore former” and the effect of U_3O_8 powder addition is a decrease in sintered density.

The sinterability of a powder can in this way be modified with addition of U_3O_8 powder, if it is too high to reach the target sintered density. The term sinterability will be defined in this report as the calculated amount of U_3O_8 powder addition given a specific sintered density and diameter shrinkage.

This report aims to investigate the properties of uranium oxide powder, as they relate to pellet quality, in the hopes of improving the efficiency of pellet manufacturing.

2 Experimental

2.1 Determination of suitable addition of U_3O_8 powder

Depending on the sinterability of a certain UO_x powder batch, different amounts of U_3O_8 powder is added to reach the target sintered pellet density. In other words, the pore forming ability of the U_3O_8 powder helps UO_x powder with high sinterability reach the target density. For UO_x powder with low sinterability less U_3O_8 powder is added. The powder batches used in the experiments were tested (pressed, sintered and evaluated) both with and without addition of U_3O_8 powder.

- A-sample: 0 w% addition of U_3O_8 powder
- B-sample: 5 w% addition of U_3O_8 powder (on UO_2 basis)

A-samples and B-samples were prepared with 0 and 5 w% U_3O_8 powder respectively (on UO_2 basis). The samples were blended, homogenized and pressed at three different pressures: 3, 4 and 5 ton/cm^2, into green pellets. The height, diameter and density of the green pellets were recorded. The green pellets were then sintered in as-close-to-production conditions as possible and the sintered pellets were again measured for height, diameter and density. The algorithm for calculating the suitable addition of U_3O_8 powder to reach the target density follows.

The pellet specification fixes the nominal dimensions of the finished sintered pellet. The powder is pressed in a die that gives the green pellet its size and shape. The pellet shrinks during sintering and the difference in green pellet diameter and nominal sintered diameter is the diameter shrinkage, se Figure 7. The desired diameter shrinkage is determined so that a suitable grinding margin is reached – around 0.05 mm on top of the nominal diameter. The diameter shrinkage [%] that gives the desired grinding margin is determined by Eq 2.

$$Ø_k = 1 - \frac{Ø_{\text{nom}} + \text{margin}}{Ø_{\text{die}}} \qquad \text{[Eq 2]}$$

The recorded density and shrinkage data were plotted against the pressure and fitted as second-degree polynomials, see Figure 8. For a predetermined pressure, the effect of 5 w% added U_3O_8 powder on the density was used to calculate the suitable amount of U_3O_8 powder add-back in order to reach the nominal target sintered density. The entire process can be followed in Algorithm 1.

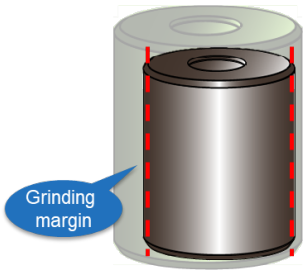

Figure 7. The green pellet shrinks during sintering. The desired diameter shrinkage includes room for a grinding margin.

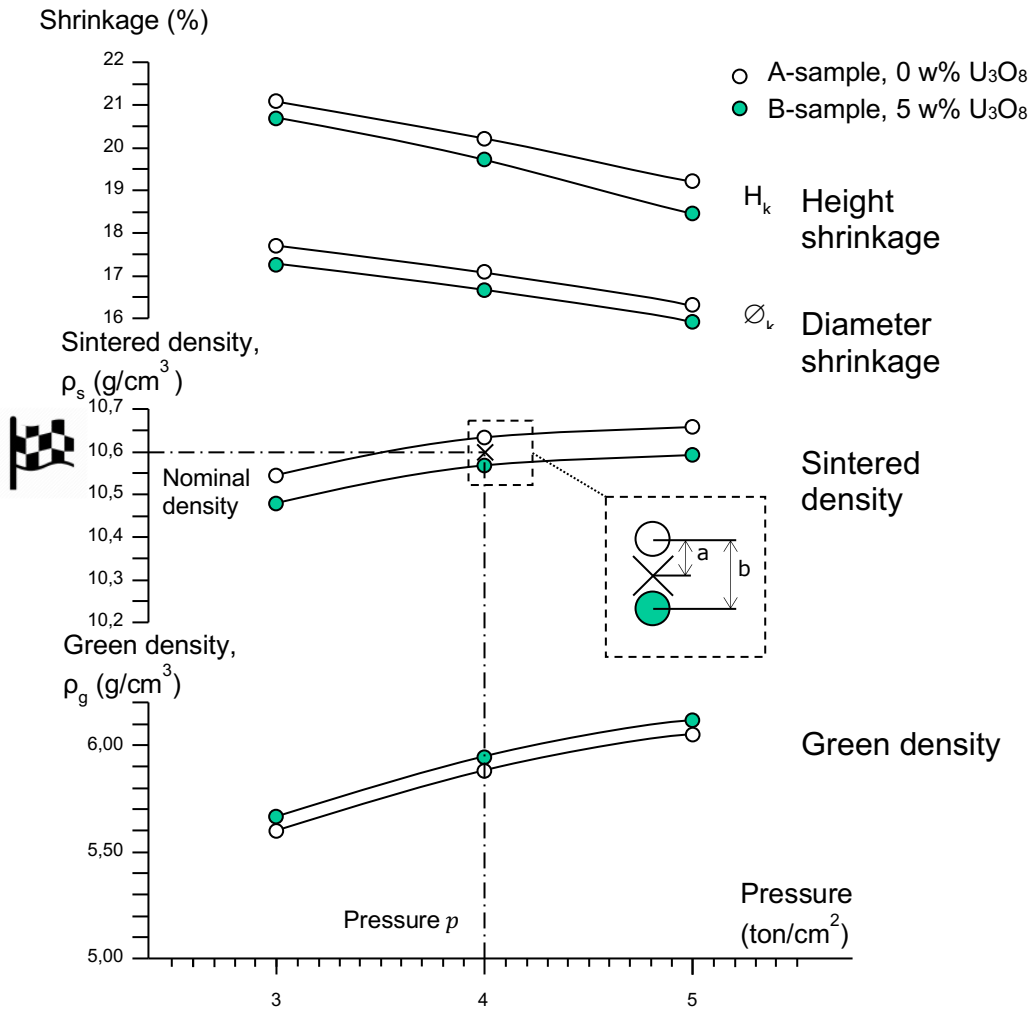

Figure 8. Shrinkages and densities as functions of pressure. The dash-dotted line shows an example of a nominal target sintered density and the pressure it takes to reach it. The distance *b* is the 5 w% U_3O_8 powder added to the B-sample, and the distance *a* is the suitable amount of U_3O_8 powder that should be added in order to reach the nominal target sintered density at this pressure.

The general process for calculating the suitable addition of U_3O_8 follows:

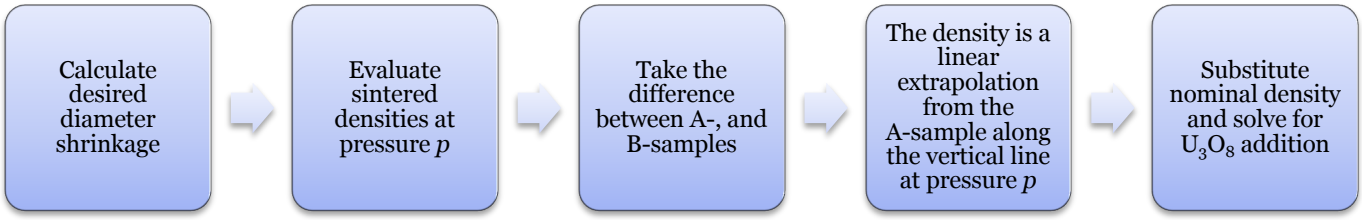

Algorithm 1. Determination of suitable addition of U_3O_8 powder.

Input: $\emptyset_{\text{nom}}$, $\emptyset_{\text{die}}$, margin, ρ_{nom}, A- and B-sample data (pressure p, sintered densities ρ_A, ρ_B)

Output: U_3O_8 powder addition to reach nominal target density

Initialization:

1. $\emptyset_k = f(\emptyset_{\text{nom}}, \emptyset_{\text{die}}, \text{margin})$
   calculate desired diameter shrinkage $\emptyset_k$, see Eq 2.

2. $\rho_{A,B} = f(p)$
   evaluate sintered densities for A-, and B-samples $\rho_{A,B}$ at pressure p, see middle section "Sintered density" of Figure 8

3. $\Delta\rho = \rho_B(p) - \rho_A(p) = b$
   take the difference in sintered density between A- and B-samples $\Delta\rho$, distance b in Figure 8

4. $\rho([U_3O_8]) = \rho_{\text{nom}} = \rho_A + \Delta\rho \cdot \frac{[U_3O_8]}{5}$
   $$\Leftrightarrow [U_3O_8] = \frac{\rho_{\text{nom}} - \rho_A}{\Delta\rho} \cdot 5 = \frac{a}{b} \cdot 5$$
   the calculated addition of U_3O_8 powder to reach nominal target density is calculated by moving along the vertical line at pressure p in Figure 8, down the distance a from the polynomial of the sintered density of the A-sample evaluated at pressure p

The aim is to maximize the reutilization of recycled UO_2 material while minimizing grinding waste. U_3O_8 powder also helps controlling the sinterability of UO_x powder by lowering the sintered density of powders with high sinterability.

2.2 Powder properties

This section explains the parameters examined and the procedures performed. Generally known empirical and theoretical relationships between process and property variables are referenced.

2.2.1 Particle size

Particle size affects sinterability in the way that the particles rearrange themselves during sintering. A powders ability to rearrange itself is a function of the surface roughness, which itself is a function of specific surface area (more on this below). Powders with a large fraction of small particles are generally less free flowing and harder to press, they form thin pore channels at the contact points between the particles and sinter to higher density. Large particles result in lower sintered density and a more homogeneous green pellet [7].

2.2.1.1 Method of measurement

The method for measuring the particle size was laser diffraction. The instrument can be run in dry or wet mode. In dry mode, agglomerates are broken up by an air stream and the particles pass through a laser beam. The incandescent laser beam is scattered on the particle surface and the scattering angle is converted into particle size in the form of an equivalent spherical diameter of a sphere with the same volume as the particle. In wet mode, the powder is dispersed in water and kept from settling by agitation. The wet mode is preferred for particles of smaller size that risk agglomeration or particles of non-free flowing powder. The values are presented as Dv10, Dv50 and

Dv90, meaning 10%, 50% and 90% of the particles respectively are smaller than the DvXX value in μm. Imagine a multi-layer sieve where only the largest particles are collected in the top sieve, 90% fall through, 50% of the particles are smaller than the middle sieve and 10% fall through the last sieve.

2.2.2 Specific surface area

Specific surface area can mostly be considered a measure of porosity, since usually the outer surface area contributes less than 10% to the total specific surface area. Specific surface area is also correlated with surface roughness, a characteristic affecting the flowability of the powder due to the friction between the particles. Voids between powder particles form pores that are enclosed during pressing of the pellet. Large pores can be eliminated by raising the pressure applied, while this effect diminishes with decreasing pore size. Small pores are instead eliminated during sintering when the particles rearrange due to diffusion [6, 10]. A low specific surface area leads to large enclosed pores and low sintered density, while a high specific surface area leads to high sintered density and a risk of cracking due to instability towards the expansion that occurs during oxidation [7]. The specific surface area has previously been shown to be related to reduction temperature in the conversion process [6].

2.2.2.1 Method of measurement

The specific surface area of the UO_x powder was measured via the BET-method, which uses the adsorption of gas molecules on a solid surface to calculate the surface area of the solid.

2.2.3 Stoichiometry – O/U ratio

The powder is stabilized during conversion after the hydropyrolysis step. Air is added in a controlled manner in order to promote passivation of the powder surface. A low stoichiometric ratio between O and U in the UO_x powder can lead to unstable powder and low sintered density [7].

2.2.3.1 Method of measurement

The O/U ratio was determined gravimetrically by weighing UO_2 powder before and after oxidization to U_3O_8 powder. The oxygen content is determined by subtraction of U and moisture content from the total mass. Since the isotopic composition can influence the mass, uranium enrichment is taken into consideration. Enrichment refers to the amount of U-235, which is the fissile material in nuclear fuel, in the UO_2 powder. See Eq 3 for calculation of the molar mass of enriched uranium. The O/U ratio is then calculated according to Eq 4, where M is molar mass and m is mass.

$$M_U = \frac{100}{\frac{(100-\text{enrichment})}{M_{U238}} + \frac{\text{enrichment}}{M_{U235}}} \quad \text{[Eq 3]}$$

$$O/U = \frac{M_U}{M_O} \cdot \frac{m_O}{m_U} \quad \text{[Eq 4]}$$

2.2.4 Bulk powder density

Bulk density is sometimes called volumetric density. The bulk density and flow rate of the powder has a negative correlation with specific surface area, and this has to do with the friction between the particles [6]. Powder particles with higher surface area has a rougher surface morphology with sharp edges which decreases the flowability of the powder. Bulk density determines how much powder is filled into the dies in the press to reach the dimensional and density specifications.

2.2.4.1 Method of measurement

The free-flowing powder is poured into a container of known volume through a funnel at 80 cm above the container, and excess powder is scraped off the top of the container. The container is weighed before and after pouring and the bulk density is calculated as the mass to volume ratio.

2.3 Pellet properties

This section describes the properties of the pellets once they are sintered, both physical and derived, that are examined in the report.

2.3.1 Pellet density – Archimedes principle

Pellet density is part of the nuclear design of the fuel. The uranium atoms need to be close enough to each other to ensure perpetuation of the nuclear reactions. The energy released in this process is transferred to the surrounding water and drives the electricity generating turbine.

2.3.1.1 Method of measurement

The sintered pellet density was measured according to Archimedes principle, which states that a body immersed in a fluid becomes lighter by an amount equal to the weight of the fluid that it has displaced. The pellet is first weighed in air and then in water. The difference in weights is the buoyancy, which is used to calculate the density. The calculations are corrected for the mean atmospheric density, and the density of water at the temperature at the time of measurement. Pellet density [g/cm3] according to Archimedes principle is calculated by Eq 5 below. The atmospheric and water densities are considered known functions of temperature.

The green pellet density was determined volumetrically by assuming a cylindrical shape, since the green pellet would fall apart if submerged in a liquid. The green pellet is weighed and measured for height and diameter. The end caps are assumed to be planar and the volume for a straight cylinder is calculated.

$$\rho = \frac{(m_{\text{dry}} * \rho_{H_2O} - m_{\text{wet}} * \rho_{\text{air}})}{(m_{\text{dry}} - m_{\text{wet}})} \qquad \text{[Eq 5]}$$

2.3.2 Relative densification

Another derived unit for sinterability is the relative densification. It compares the pressed green density with the sintered and theoretical densities. Natural uranium consists mostly of the heavier U-238 nuclide but since the UO_2 often is enriched with the fissile U-235 nuclide, enrichment is taken into account. The theoretical density is calculated as Eq 6 with the data in Table 1, and the relative densification is calculated as Eq 7.

Table 1. Theoretical densities for UO_2 if all the atoms in the molecule were of either nuclide [11].

Theoretical density [g/cm^3]	
$U(238)O_2$	$U(235)O_2$
10.96	10.838

$$\rho_{TD} = \frac{\rho_{U(238)O_2}\cdot(100-\text{enrichment})+\rho_{U(235)O_2}\cdot\text{enrichment}}{100} \quad \text{[Eq 6]}$$

$$\text{relative densification} = \frac{\rho_s-\rho_g}{\rho_{TD}-\rho_g} \quad \text{[Eq 7]}$$

2.3.2.1 Method of measurement

The method of measuring the density is the Archimedes principle for sintered pellets and volumetric for green pellets.

2.3.3 Equivalent moisture content – hydrogen content

Hydrogen accumulated in the pellet can react with the zirconium in the fuel rod and lead to embrittlement of the material.

2.3.3.1 Method of measurement

The hydrogen content in the pellets was examined by heat extraction, where argon as a carrier gas drives off impurities such as nitrogen, oxygen and hydrogen gas at around 2 000°C. Molecular sieves separate the different impurities and the difference in gas thermal conductivity relative to the reference carrier gas is detected and interpreted as concentration.

2.4 Oxidation of UO_2 by H_2O_2 – oxidation mechanisms and the Ghormley tri-iodide method

To determine the chemical activity of a UO_2 powder it was oxidized by H_2O_2. H_2O_2 can react with oxide surfaces via two mechanisms: two-electron transfer redox reactions, or catalytical decomposition of H_2O_2 without oxidizing the surface [12]. The redox reactions of H_2O_2 oxidizing U(IV) to U(VI) are described by Eq 8 and the catalytic decomposition of H_2O_2 adsorbed on UO_x surface by Eq 9.

$$\begin{gathered} UO_2 + H_2O_2 \rightarrow UO_2^+ + HO^\bullet + HO^- \\ UO_2^+ + HO^\bullet \rightarrow UO_2^{2+} + HO^- \end{gathered} \quad \text{[Eq 8]}$$

$$\begin{gathered} H_2O_2(\text{ads}) \rightarrow 2HO^\bullet(\text{ads}) \\ H_2O_2(\text{ads}) + HO^\bullet(\text{ads}) \rightarrow H_2O(\text{ads}) + HO_2^\bullet(\text{ads}) \\ 2HO_2^\bullet(\text{ads}) \rightarrow H_2O_2 + O_2 \end{gathered} \quad \text{[Eq 9]}$$

The concentration of H_2O_2 as a function of time was determined by the Ghormley tri-iodide method [13, 14]. KI is added as an indicator and the I^- is oxidized to I_3^- by the H_2O_2 left in the solution after reacting with the UO_x. The absorbance of I_3^- can be detected spectrophotometrically at around 360 nm and is proportional to the concentration of H_2O_2. The tri-iodide in the Ghormley tri-iodide method forms according to Eq 10.

$$\begin{gathered} 2I^- + H_2O_2 \rightarrow I_2 + 2OH^- \\ I_2 + I^- \rightarrow I_3^- \end{gathered} \quad \text{[Eq 10]}$$

2.5 Material selection, treatment, and equipment used

All the UO_x powder used in the present work was produced by Westinghouse Electric Sweden AB in Västerås. The chemical and physical properties of the powders were examined on site at Westinghouse's facilities.

UO_x powder particle size was measured by laser diffraction on a Malvern Mastersizer 3000. The measuring range of the instrument was 0.01–3 500 µm and the standard deviation was about ±0.2 µm for particles around 20 µm. The

specific surface area was measured by BET on a Micrometrics TriStar II 3020, with a measuring range of 5–22 m^2 total area and an absolute error of ±0.3 m^2/g. Determination of stoichiometric O/U ratio was performed by oxidation of UO_2 to U_3O_8 at 900°C. The method admits a precision of ±0.02% for U content, and at worst ±0.003 absolute for O/U ratio, at 95% confidence level. The density measurements were performed on weighing and scaling equipment to a precision of at least ±0.03 g/cm^3.

All powders were weighed to an accuracy of 10^{-5} kg on a Mettler AT 200, AG 204, AE 50, alternativity AX204 microbalance. The powders to be blended were sifted through a 200 µm sieve and homogenized in plastic bottles in a Turbula shaker mixer for 60 minutes. All mass fractions of blended powders with U_3O_8 powder additions were calculated on a UO_2 basis. The powders and blended powders were pressed on a manually loaded hydraulic press, at around 4 and 5 ton/cm^2, into green pellets. The physical dimensions of the pellets (height and diameter) were recorded with digital calipers with an accuracy of 10^{-5} m. The green densities of the pellets were calculated through the assumption of a cylindrical shape. The green pellets were then sintered in an H_2 atmosphere with small additions of CO_2 in a five heat zones sintering furnace, see Table 2.

Table 2. Sintering furnace heat zones, temperatures in °C.

Low temperature zone [°C]	High temperature zone [°C]
Zone 1–Zone 2	Zone 3–Zone 5
400–800	1000–2000

2.6 Data analysis – apparent trends in production parameters

Historical production data was examined for trends in powder properties and sinterability. The database of tracked production parameters of UO_2 powders, produced between 2018 and 2019 that were not blended (i.e. any pellets produced from a single batch of UO_2 powder), was analyzed for trends regarding sinterability. Production and material parameters that were considered include: U_3O_8 powder addition, equivalent moisture content, O/U, bulk density, specific surface area, trace impurities (Al, Cr, F, Fe), particle size and relative densifications of powders with and without added U_3O_8 powder.

To look for trends in production parameters as they affect sinterability, U_3O_8 powder addition was chosen as response variable with the idea that increasing U_3O_8 powder addition indicates higher sinterability of a UO_x powder. A matrix plot of all parameters was visually examined for apparent trends, see Figure 10. To avoid correlations between predictor variables, meaning several variables explain the same phenomenon (so called *multicollinearity*), pairwise plots are shown in the matrix. In Figure 10 for example, Dv10 and Dv50 seem to be linearly correlated so including both variables does not add more information.

With the help of statistical software algorithms, various regressions of the data were made. A best subsets regression is an iterative method to determine a regression model of the fitted data. It finds the best one-variable, two-variable, three-variable, and so on, model with the best fit and smallest error. This is a non-physical approach, or a black box approach, to the data analysis. Using fewer variables is desirable because of simplicity, however the model still must have a good fit.

A stepwise selection of terms regression is another iterative method. It adds one variable at a time, considering the statistical p-value according to a heuristic algorithm.

2.7 Varying U_3O_8 powder batch

In order to assess the influence on sinterability of the U_3O_8 powder, one batch of UO_2 powder was blended with 6 different U_3O_8 powder batches at 5 w% addition, see Table 3. The blended powders were assessed according to the algorithm in Section 2.1.

Table 3. UO_2 batch number 1051749 was used with addition of 5 w% (on UO_2 basis) of 6 different U_3O_8 powder batches.

Sample ID	1B	2B	3B	4B	5B	6B
UO_2 batch	1051749	"	"	"	"	"
U_3O_8 batch	1049479	1051877	1051269	1051475	1051600	1050524

Table 4. Powder properties for UO_2 powder varying U_3O_8 powder batch.

Batch	O/U	BET [m^2/g]	Dv10 [µm]	Dv50 [µm]	Dv90 [µm]
1051749	2.14	5.72	8.84	20.40	46.10

2.8 Blending powders of high/low sinterability

UO_2 powders with a suitable amount above 8 w% U_3O_8 powder to reach its target sintered density were called active powders. Similarly, UO_2 powders with determined addition of less than 3 w% U_3O_8 powder were called inactive powders.

- High sinterability – *active* powder: >8 w% U_3O_8 powder addition
- Low sinterability – *inactive* powder: <3 w% U_3O_8 powder addition

To evaluate the effect of blending powders on various powder and pellet properties, combinations of active and inactive powders in different constellations were blended and assessed according to the algorithm in Section 2.1, see Table 5.

The experiment was performed as follows: equal mass amounts of virgin UO_2 powders were weighed and homogenized with addition of 0, 5, and 10 w% U_3O_8 powder (on UO_2 basis). For each combination of blended powders, 8 pellets were pressed at around 4, and 5 ton/cm^2. The height, diameter and density of the green pellets were calculated and evaluated. The 5 most similar of these were selected to be sintered.

The blended powders were analyzed in the laboratory for particle size and specific surface area.

Table 5. Virgin UO_2 powders (active and inactive) and the blended combinations.

Virgin UO_2 powders \ Blended powders		A2 active/ active	B2 active/ active	C2 active/ active	D2 active/ inactive	E2 active/ inactive	F2 active/ inactive	G2 inactive/ inactive
1051469	active	x	x		x			
1051750	active	x		x		x		
1048957	active		x	x			x	
1051233	inactive				x	x	x	
1051599	inactive							x
1051466	inactive							x

2.9 Chemical activity of UO_2 powder by oxidation with H_2O_2

Standard solutions were made of:

- 10 mM Na_2CO_3 (CAS[497-19-8]), pH-adjusted to 8.2 with HCl and purged with N_2 gas
- 1 M $NaOOCCH_3$ (CAS[127-09-3]),1 M $HOOCCH_3$ (CAS[64-19-7]) used as pH-buffer, with addition of (2 drops in 10 ml buffer) 3% ammonium-heptamolybdate ($(NH_4)_6Mo_7O_{24}$) (CAS[12054-85-2]) used as catalyst
- 1 M KI (CAS[7681-11-0]) used as indicator in Ghormley's tri-iodide method

Calibration curves for H_2O_2 concentration (H_2O_2 30% provided by Merck (CAS[7722-84-1])), using the 10 mM Na_2CO_3 standard solution as well as water, were made with 0.00125, 0.00375 0.0100, 0.0250 mM estimated H_2O_2 concentrations at wavelength 360 nm on a Shimadzu UV-1800 UV-spectrophotometer. A background reference cuvette was measured containing 10 mM Na_2CO_3 solution.

UO_2 powder was added to 50 ml 10 mM purged Na_2CO_3 pH 8.2, such that the total specific surface area added summed 0.5 m^2/50 ml, meaning around 0.1 g powder depending on the powder batch properties, and a specific surface area to volume ratio S_A/V around 10 000 m^{-1}. The UO_2 powder was washed 3 times in 50 ml 10 mM purged Na_2CO_3 adjusted to pH 8.2, stirred for 30 minutes, let settle for 15 minutes and the liquid decanted by pipette. The bottom part, about 5 ml solution with suspended powder, was left in the beaker after each washing to make sure no uranium was removed. The magnetic stirrer was always set to the same speed. The solution was then prepared with H_2O_2 to its initial concentration of around 0.025 mM and the beaker was covered to prevent ambient UV-light breakdown of H_2O_2.

A timer was started as soon as the H_2O_2 was added. After 30 seconds, the first aliquot was taken to record the initial H_2O_2 concentration (absorbance at 360 nm after 1 M KI and catalyst added according to the Ghormley tri-iodide method). Every 20 minutes an aliquot was taken and evaluated for H_2O_2 concentration. About 1 ml was filtered through a 0.2 µm acetate syringe filter to remove all particles and stop the oxidation. Out of the aliquot, 0.8 ml was pipetted into a cuvette, together with 0.1 ml pH-buffer with the catalyst, 0.1 ml 1 M KI and 1.0 ml water to reach 2.0 ml total in the cuvette. Three readings were made on the spectrophotometer after a reaction time in the cuvette of 2 min ± 2 s. After about 3 hours, the change in H_2O_2 concentration approached zero.

2.10 Visual inspection of UO_2 and U_3O_8 powders via SEM

The UO_2 powders were analyzed via Scanning Electron Microscopy (SEM). It produces a focused electron beam that interacts with the atoms of the sample and gives information on the surface topography with a magnification between roughly 200×–10 000×.

Several powders were analyzed on a Thermo Fisher Scientific Phenom Pro Desktop Scanning Electron Microscope. Images of the powders were stored at 9 different magnifications (275×, 400×, 650×, 900×, 1 250×, 2 300×, 3 500×, 6 000×, 8 600×). The powders were fixed on carbon conductive tabs. The SEM was run at 10 kV accelerating voltage.

3 Results and discussion

3.1 Determination of suitable addition of U_3O_8 powder

The powders were pressed with a 5 w% U_3O_8 powder addition at 3 different pressures, and evaluated at one, predetermined pressure. Previously the diameter shrinkage was calculated but not taken into account regarding the determination of suitable addition of U_3O_8 powder.This lead to unpredictable results and increased grinding waste. The algorithm to calculate the proper addition was changed from using the predetermined pressure to dynamically take the diameter shrinkage into account when determining the pressure, see Algorithm 2.

Eq 2 shows how the desired diameter shrinkage is related to the pellet specification. Shrinkage and pressure are correlated such that higher pressure leads to less shrinkage. To reach the nominal diameter $Ø_{nom}$ plus the grinding margin, each powder batch thus has an optimal pressure to reach the desired diameter shrinkage.

From the sintered density as function of shrinkage, the optimal shrinkage to reach both the desired diameter plus grinding margin and nominal density ρ_{nom} is obtained. For the powder batch being tested, the desired diameter shrinkage leads to certain sintered densities of the A- and B-samples ρ_A, ρ_B (0 and 5 w% U_3O_8 added respectively), as interpolated on the polynomials. The same sintered densities as functions of pressure numerically give the pressure at which the desired diameter shrinkage occurs.

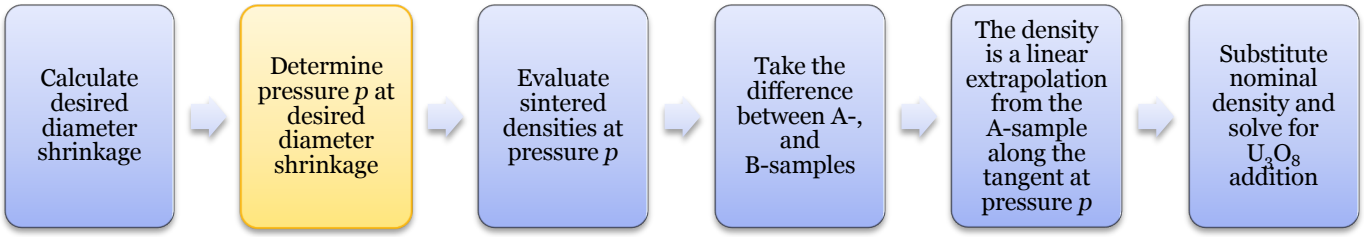

Algorithm 2. Author's suggestion of how to determine proper addition of U_3O_8 powder.

Input: $\emptyset_{nom}, \emptyset_{die}$, margin, ρ_{nom} , A- and B-sample data (pressure p, sintered densities ρ_A, ρ_B)

Output: U3O8 powder addition to reach nominal target density

Initialization:

1. $\emptyset_k = f(\emptyset_{nom}, \emptyset_{die}, \text{margin})$
   desired diameter shrinkage $\emptyset_k$, see Eq 2

2. $\rho_{A,B} = f(\emptyset_k); \rho_{A,B} = f(p)$
   sintered densities $\rho_{A,B}$ as functions of desired diameter shrinkage and pressure

3. $p = f\left(\rho_{A,B}(\emptyset_k), \rho_{A,B}(p)\right)$
   pressure p at which desired diameter shrinkage occurs, *author's addition*

4. $\Delta\rho = \rho_B(p) - \rho_A(p)$
   difference in sintered density between A- and B-samples $\Delta\rho$ at pressure p

5. $\rho([U_3O_8]) = \rho_{nom} = \Delta\rho \cdot \frac{[U_3O_8]}{5} + \rho_A$
   $$\Leftrightarrow [U_3O_8] = \frac{\rho_{nom} - \rho_A}{\Delta\rho} \cdot 5$$
   calculated amount addition of U_3O_8 powder to reach nominal target density

Step 3 in Algorithm 2 was an addition by the author to combine both diameter shrinkage and pressure where before either parameter was used separately.

3.2 Data analysis – apparent trends in production parameters

Logged process parameters from UO_2 pellet production were analyzed for trends regarding sinterability. Using the calculated U_3O_8 powder addition as a measure of sinterability, the phenomenon was investigated as a function of various parameters. The results show that a single parameter alone cannot easily explain sinterability. In Figure 10 the top row shows X-Y plots of response variable U_3O_8 powder addition as a function of the various predictor variables. The rows below are pairwise X-X plots of the predictors. Figure 9 highlights a few X-Y plots, marking the difficulty in appointing a single parameter that explains sinterability.

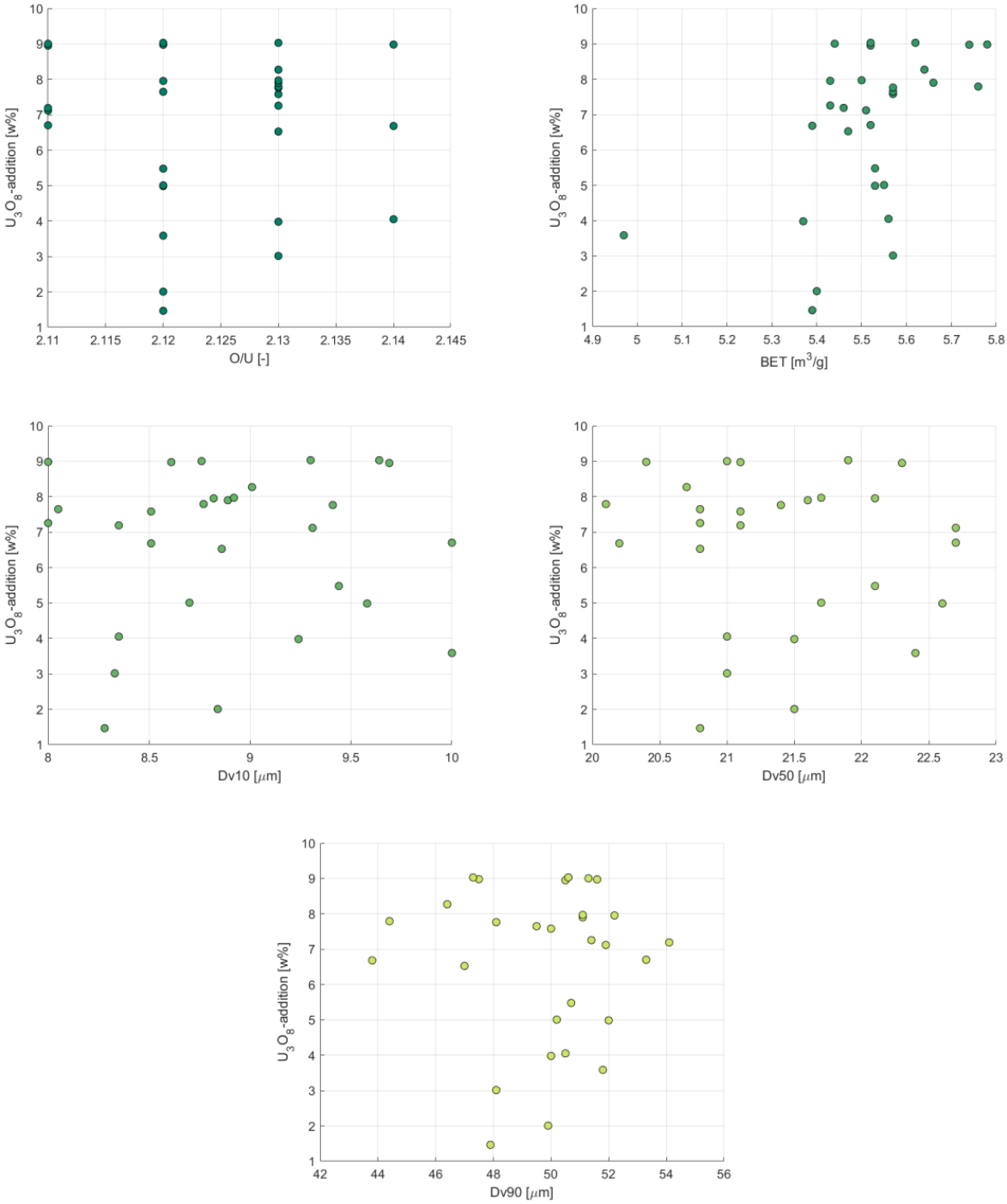

Figure 9. Calculated U_3O_8 powder addition as a function of various parameters.

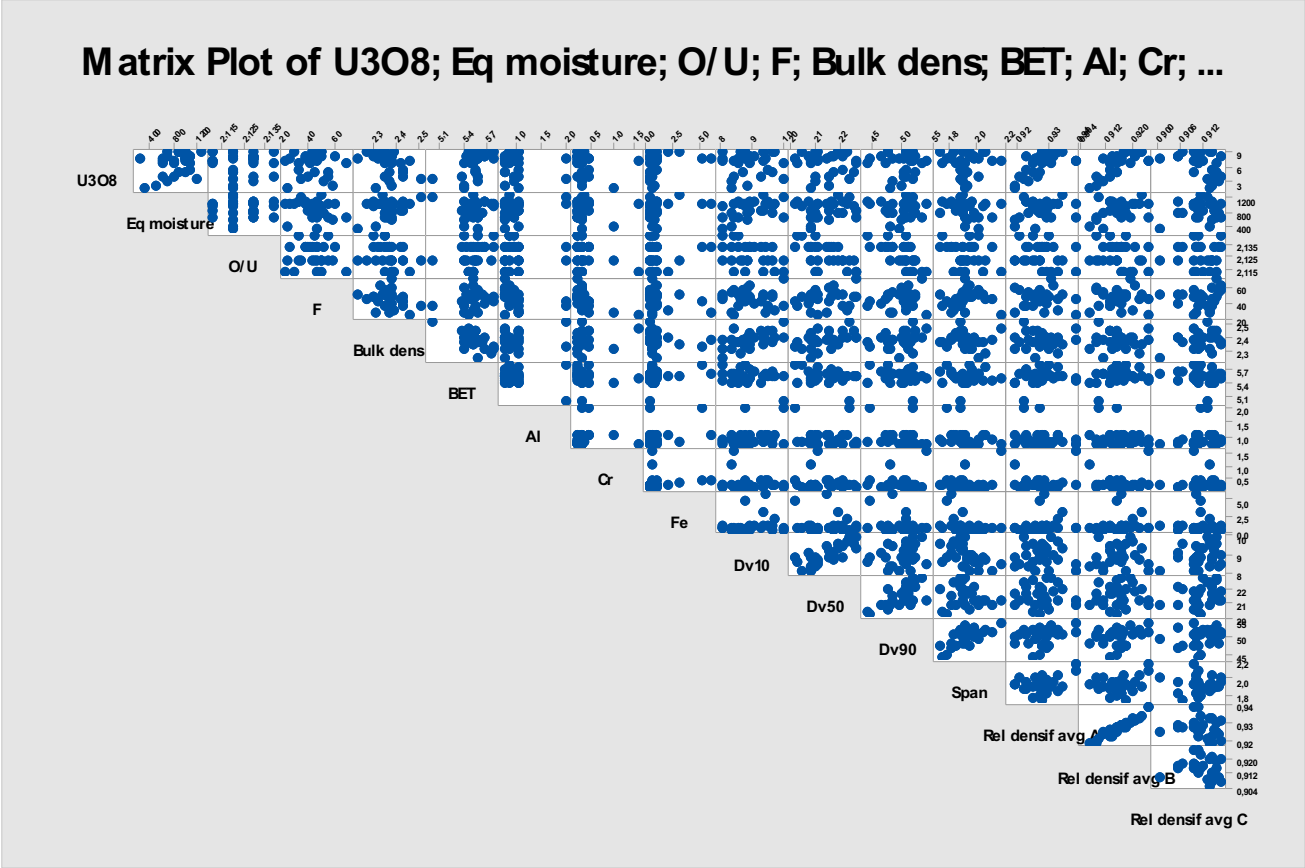

Figure 10. Matrix plot of process parameters. First row is X-Y plots of each parameter vs the response U_3O_8 powder addition. Rows below are X-X plots of parameters vs each other for multicollinearity check.

Table 6. Best subsets regression with U_3O_8 powder addition as response and various process parameters as predictor variables. The table lists the regression models that minimize the total error S, including more variables each iteration. The bolded line coincides with the model found by the stepwise selection of terms method.

Vars	R-Sq	R-Sq (adj)	R-Sq (pred)	Mallows Cp	S	Eq moisture	O/U	F	Bulk dens	BET	Al	Cr	Fe	Dv10	Dv50	Dv90	Span	Rel dens f avg A	Rel dens f avg B	Rel dens f avg C
1	52.2	50.5	42.1	62.5	1.5614														X	
1	45.2	43.2	32.0	75.3	1.6723													X		
2	70.0	67.7	61.2	32.0	1.2618														X	X
2	64.4	61.6	52.9	42.3	1.3745				X										X	
3	78.2	75.6	71.9	18.9	1.0964							X							X	X
3	76.0	73.1	64.5	23.0	1.1509					X									X	X
4	82.1	79.1	72.4	13.8	1.0145				X					X					X	X
4	82.0	79.0	73.7	14.0	1.0170	X			X										X	X
5	86.1	83.0	79.6	8.5	0.91384	X			X			X							X	X
5	85.8	82.8	78.8	8.9	0.92117	X			X					X					X	X
6	**87.8**	**84.5**	**76.5**	**7.3**	**0.87286**	**X**			**X**			**X**		**X**					**X**	**X**
6	87.3	83.8	54.8	8.3	0.89316			X	X			X		X					X	X
7	88.9	85.2	60.8	7.4	0.85444	X		X	X			X		X					X	X
7	88.5	84.7	78.7	8.1	0.86878	X			X	X		X		X					X	X
8	90.2	86.3	62.9	6.9	0.82113			X	X			X			X	X	X		X	X
8	89.5	85.3	63.6	8.2	0.85028	X		X	X	X		X		X					X	X
9	91.5	87.5	69.4	6.6	0.78513			X	X	X		X			X	X	X		X	X
9	91.2	87.0	67.9	7.2	0.80072			X	X			X		X	X	X	X		X	X
10	92.5	88.3	75.0	6.8	0.75954			X	X	X		X		X	X	X	X		X	X
10	92.0	87.5	71.6	7.7	0.78460			X	X			X		X	X	X	X	X	X	X
11	92.8	88.2	75.7	8.1	0.76165			X	X	X		X		X	X	X	X	X	X	X
11	92.6	87.8	73.1	8.6	0.77498	X		X	X	X		X		X	X	X	X		X	X
12	92.9	87.5	71.0	10.0	0.78328		X	X	X	X		X		X	X	X	X	X	X	X
12	92.9	87.5	72.6	10.1	0.78356			X	X	X	X	X		X	X	X	X	X	X	X
13	92.9	86.7	66.9	12.0	0.80769		X	X	X	X	X	X		X	X	X	X	X	X	X
13	92.9	86.7	67.9	12.0	0.80894		X	X	X	X		X	X	X	X	X	X	X	X	X
14	92.9	85.8	62.6	14.0	0.83599		X	X	X	X	X	X	X	X	X	X	X	X	X	X
14	92.9	85.8	59.0	14.0	0.83601	X	X	X	X	X	X	X		X	X	X	X	X	X	X
15	92.9	84.7	50.0	16.0	0.86753	X	X	X	X	X	X	X	X	X	X	X	X	X	X	X

The regression analyses suggest the model described in Eq 11, with the statistics given in Table 6 on the bolded line. See Table 7 for a variable key and where to read more about each.

$$U_3O_8 = 6.618 + 0.494 \cdot \text{Eq moisture} - 0.797 \cdot \text{Bulk dens} - 0.352 \cdot \text{Cr} + 0.393 \cdot \text{Dv10} + 1.353 \cdot \text{Rel densf avg B} - 0.866 \cdot \text{Rel densf avg C} \quad \text{[Eq 11]}$$

Table 7. Variable key

Variable	Explanation of variable	Further information
Eq moisture	Equivalent moisture content – hydrogen content	Section 2.3.3
O/U	Stoichiometry – O/U ratio	Section 2.2.3
Bulk dens	Bulk powder density	Section 2.2.4
BET	Specific surface area	Section 2.2.2
Al, Cr, F, Fe	Element content	
DvXX, Span	Particle size	Section 2.2.1
Rel densf avg X	Relative densification	Section 2.3.2

No clear single parameter (or combinations of parameters) relationships were discovered. In the future, a designed experiment would likely be a better approach to analyze process data – especially for contradictory powders e.g. with high specific surface area but low sinterability and vice versa. Traceability of the powders and the process parameters utilized in the production was important for mapping data to a specific batch. Blended powders quickly lose the connection to the utilized process parameters and individual powder properties, as shall be further demonstrated in Section 3.4.

A machine learning approach to the data analysis of production parameters is planned. Again, the quality of the data is of great importance even for advanced algorithms.

3.3 Varying U_3O_8 powder batch

One UO_2 powder batch was blended with 5 w% of 6 different U_3O_8 powder batches. The sintered density of each blended powder as a function of green density is shown in Figure 11, and the diameter shrinkage after sintering as a function of green density in Figure 12. When considering the sintered density, not much difference can be noted. However, there is one U_3O_8 powder batch that stands out as it deviates around 1.5 percentage points from the rest with regard to diameter shrinkage.

The data points cluster into groups corresponding to the 3 different pressure used while pressing the pellets, where higher pressure leads to higher densities (green and sintered).

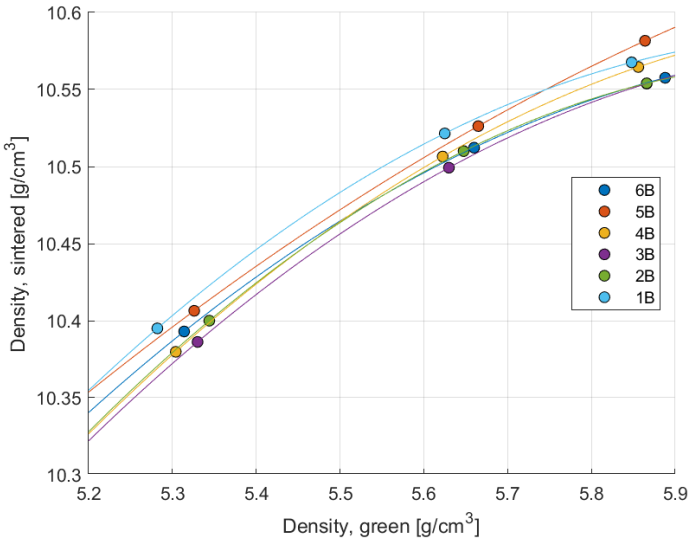

Figure 11. Sintered density as a function of green density of blended powders of varying U_3O_8 powder batch. All blended powders were within the margin of error.

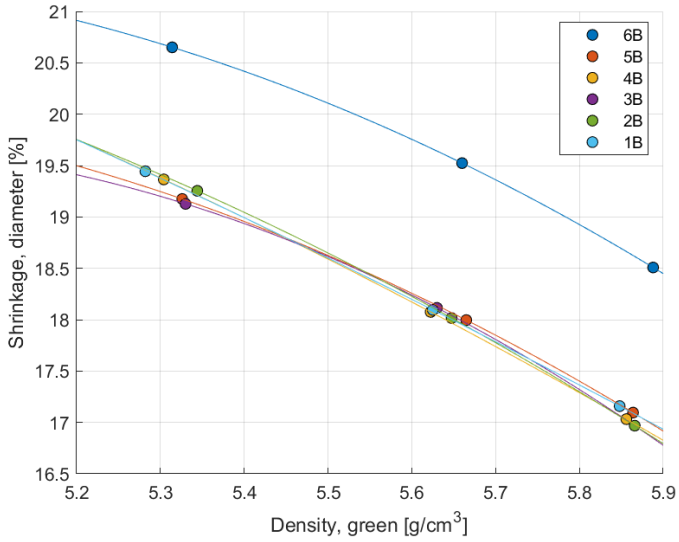

Figure 12. Diameter shrinkage as a function of green density of blended powders of varying U_3O_8 powder batch. One batch (6B) stands out with a higher shrinkage than the others.

The reason for the deviating shrinkage is unknown since no historical data on U_3O_8 powder properties were recorded. The blended powder combination 6B has a higher shrinkage, meaning it risks not being ground to the correct diameter.

3.4 Blending powders of high/low sinterability

Powders of high and low sinterability were blended in equal mass proportions in different combinations. The blended powder and the green and sintered pellet properties were characterized with and without U_3O_8 powder addition. See Table 3 for a summary of blended powder compositions.

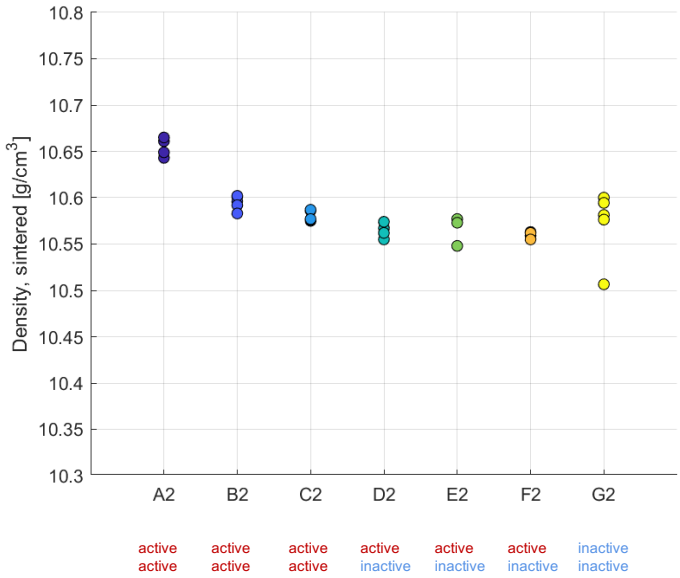

Figure 13. Sintered density of the blended powders A2–G2, pressed at 4 ton/cm² without U_3O_8 powder addition. Five pellets of each blended powder were sintered and evaluated.

The sintered density should, in theory, increase with sinterability and thus blending with inactive powder should decrease the density. This cannot be clearly seen in Figure 13. Especially sample G2 is shown to increase in sintered density even though it consists of two inactive powders. For the case of the active/active blend A2 there is an increase in sintered density. A more detailed examination of the sintered density for each blended powder compared to the virgin powders follows.

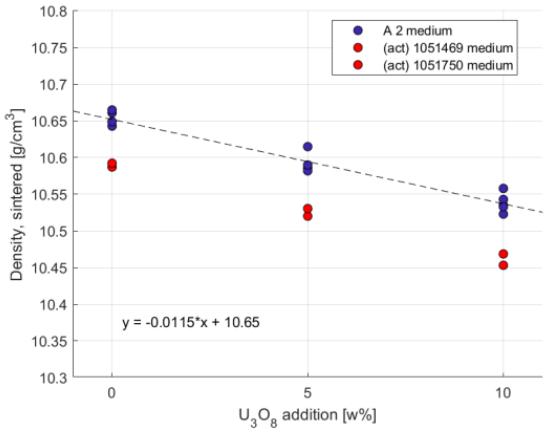

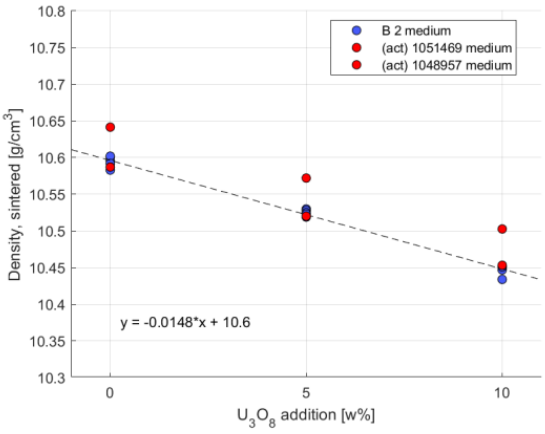

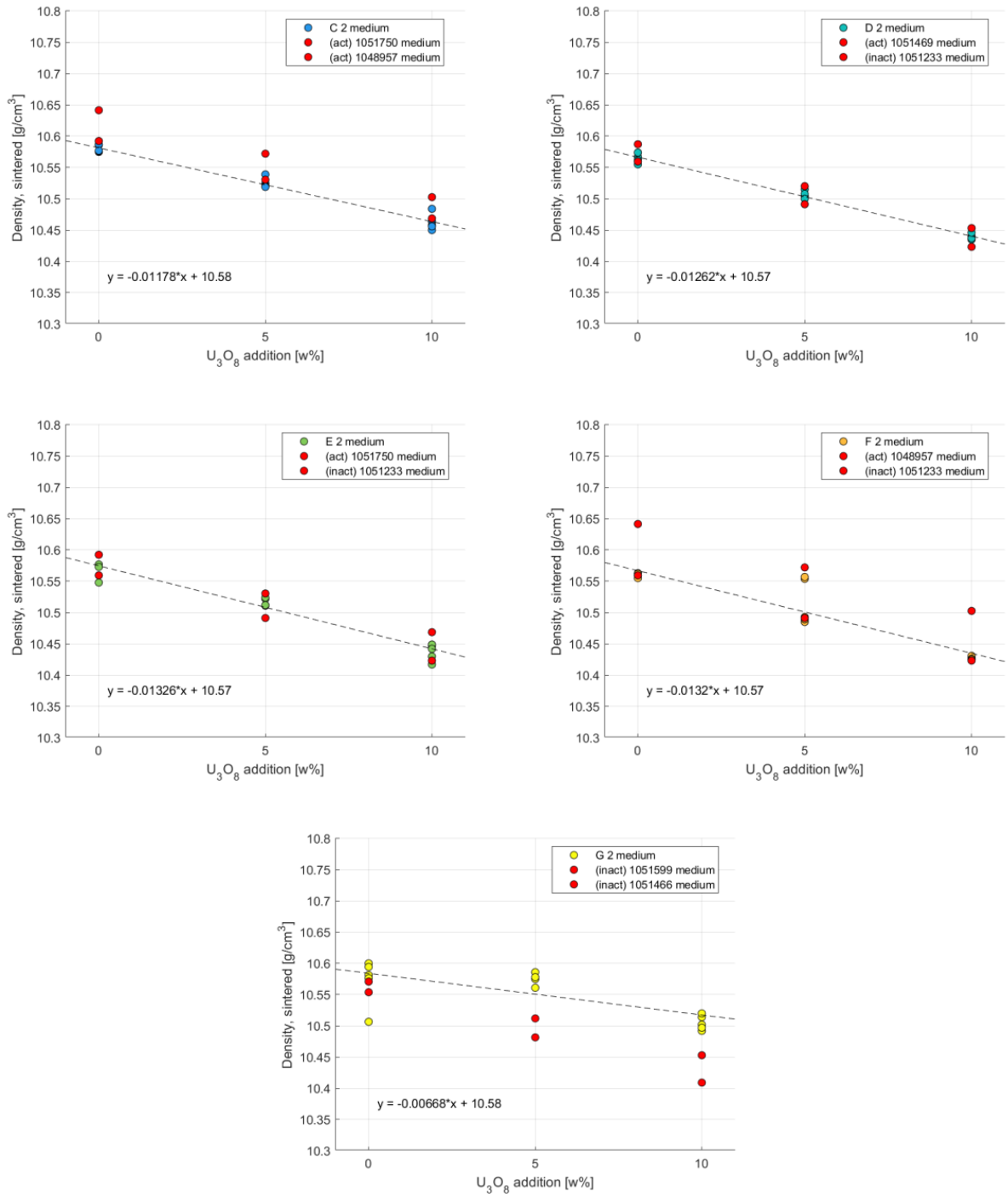

Figure 14. Sintered density [g/cm³] as a function of U_3O_8 powder addition for the active/inactive blended powders compared to the virgin powder constituents, pressed at 4 ton/cm² without U_3O_8 powder addition. The dashed lines are fitted to the sintered densities of the blended powders as a linearly regressed function of U_3O_8 powder addition. The coefficients are shown in the equation inserted in the diagrams.

It can be seen in Figure 14 that the sintered densities of the blended powders mostly follow the sintered density of the virgin powders, except for previously mentioned samples A2 and G2 where the blended powders increase in

sinterability compared to the virgin powders. Sample G2 especially shows a poor fit to the linear regression with respect to U_3O_8 powder addition.

Other properties that were examined for the blended powders were specific surface area, particle size and U_3O_8 powder addition according to the evaluation of sinterability.

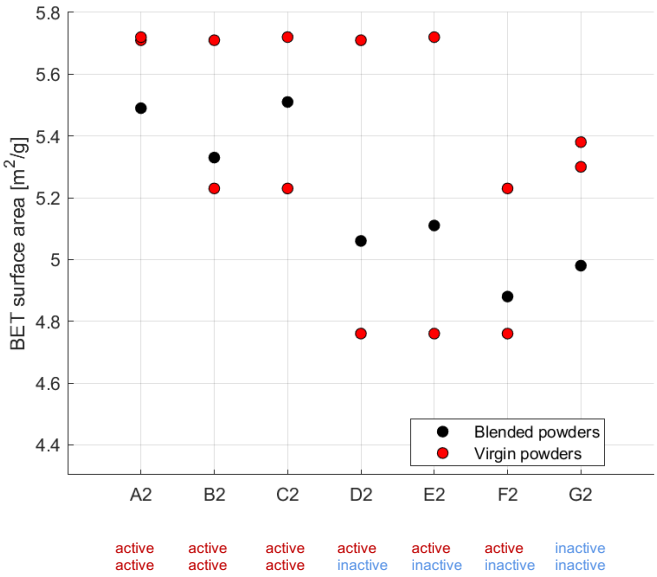

Figure 15. Specific surface area [m²/g] for blended active/inactive powders and their virgin powders.

For many properties it can be expected that the blended powders behave as the mean of the virgin powders that make up the blend. For the specific surface area, around 90% of the contribution to the surface area comes from pores inside the powder particles. Hence, the outer surface area of the particles, and thus particle size, will not influence the specific surface area much. Even if the action of blending the powders alters the particle size distribution (e.g. by fracturing particles or creating agglomerates) it should not particularly affect porosity and specific surface area. However, the specific surface area measurements of the blended powders do not always align with the mean of the virgin powders. It can be seen in Figure 15 that the specific surface area of the blended powders often ends up below the mean of the virgin powders, or even below that of the virgin powders themselves – indicating that the porosity of the blended powders has decreased.

This may be due to how the specific surface area is averaged over a sample. Only one value for specific surface area is reported for each powder, nothing is known about the distribution of the specific surface area over e.g. the different particle size fractions, more on this below.

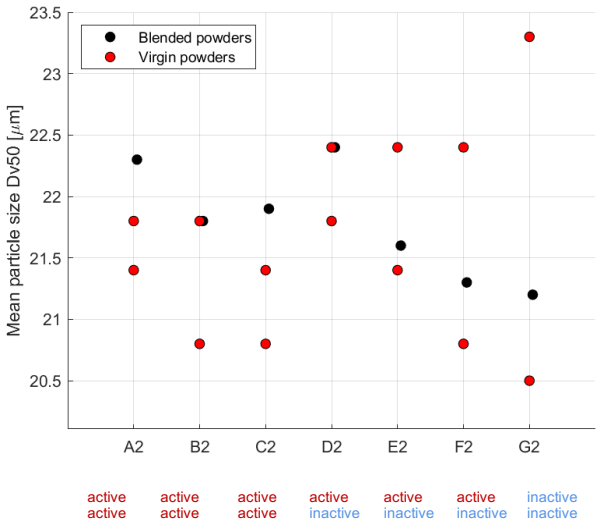

Figure 16. Mean particle size Dv50 [µm] for blended active/inactive powders and their virgin powders.

For mean particle size Dv50, in Figure 16, the values deviate both above and below the mean and the virgin powder particle sizes. This can be due to the virgin powders having different distributions of particle sizes. One might have a large tail of small particles while another might have a larger fraction of large particles. Mixing these will shift the mean particle size in different directions.

It should also be noted that the DvXX values are spherical approximations of the real particle size. The equivalent volumetric particle size may differ depending on how the incandescent light hits the particle during laser diffraction. A projection image is taken to represent the particle and the equivalent diameter of a sphere occupying the same space is reported. This makes the DvXX value sensitive to particle shape. See Figure 19 for a visual example of UO_2 particles. The particles are often oval shaped rather that spherical meaning the particle size might be over- or underestimated.

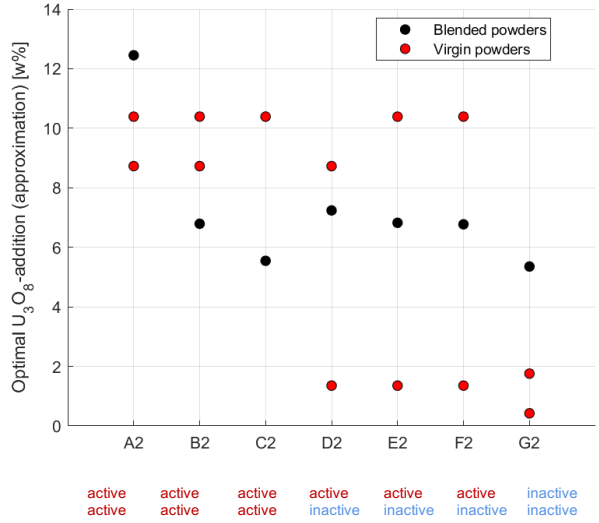

Figure 17. Calculated U_3O_8 powder addition [w%] for blended active/inactive powders and their virgin powders.

An approximation of the determination of U_3O_8 powder addition – only considering one pressure instead of 3 different pressures otherwise used in Algorithms 1 and 2 – shows that the optimal U_3O_8 powder addition tends to even out for all blends except for A2 (active/active) which is about twice as high as the rest, including 2 more active/active blends B2 and C2, as seen in Figure 17.

Blends A2 and G2 both turn even more active than their virgin constituents. What A2 and G2 have in common is that both result in lower specific surface area, in higher sintered density and thus in higher sinterability or U_3O_8 powder addition than their respective virgin powders. This goes against the theory that higher specific surface area leads to higher sinterability.

One hypothesis worth testing would be if it is possible to predict an increase in sinterability if the specific surface area of a blended powder is lower than that of its constituent virgin powders. The tendency for particle size predicting sinterability is not as apparent, but a larger number of samples is needed to confirm.

3.5 Chemical activity of UO_2 powder by oxidation with H_2O_2

UO_2 powder was oxidized by H_2O_2 to determine the chemical activity. The consumption of H_2O_2 was measured over time, in 20-minute intervals for 180 minutes total. The powders were washed 3 times in Na_2CO_3 pH 8.2, before addition of H_2O_2. Visual observation during the washing showed that the solution containing the inactive UO_2 powder batch 1051233 was colored a dark yellow even after a settling time of >15 min, while the solution containing the active UO_2 powder batch 1052445 was clear. The properties of the UO_2 batches can be seen in Table 8.

Table 8. Properties of the UO_2 powders oxidized by H_2O_2 in determining the chemical activity.

UO_2 batch	Mass [g]	BET [m^2/g]	U_3O_8 [w%]	Dv50 [µm]	S_A/V [m^{-1}]	O/U
1051233	0.1050	4.76	0.5%	22.40	9 996	2.10
1052445	0.0893	5.60	15.5%	20.60	10 002	2.13

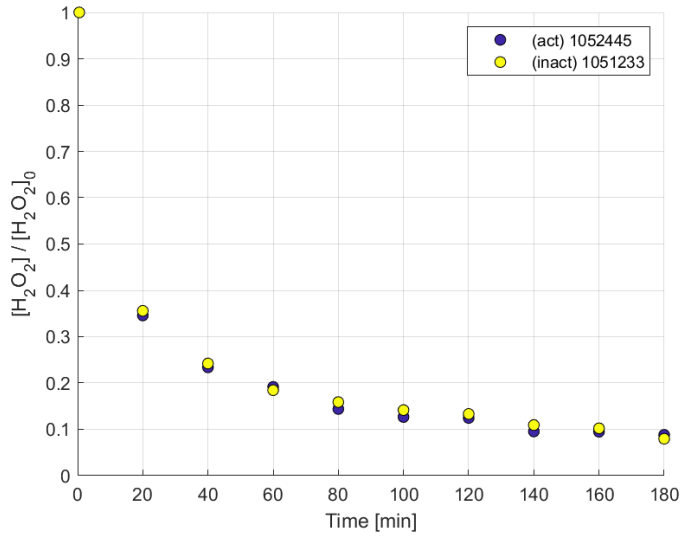

Figure 18. Normalized concentration of H_2O_2 as a function of reaction time. Initial H_2O_2 concentration was 0.025 mM.

The consumption of H_2O_2 is fast in the beginning and decreases with time, as can be seen in Figure 18. For an equal specific surface area to solution volume ratio S_A/V, the rate of consumption is equal.

3.6 Visual inspection of UO_2 and U_3O_8 powders via SEM

A library of SEM images of UO_2 and U_3O_8 powders, at various magnifications, was developed. Following are examples of images obtained by the SEM of UO_2 and U_3O_8 powders and some of their properties. Figure 19 shows the difference between UO_2 particles and U_3O_8 particles. The particle size and morphology differ considerably. The UO_2 particles are large and smooth in comparison to the U_3O_8 particles, which are small and sharp.

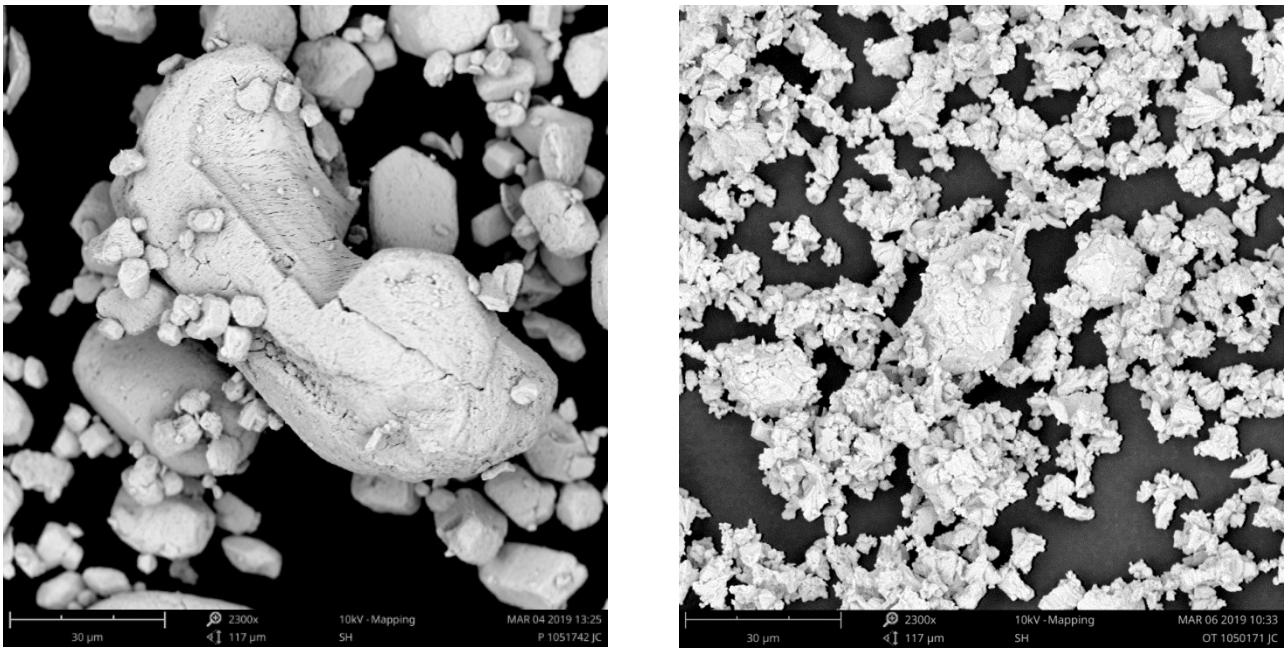

Figure 19. SEM image of UO_2 (left) and U_3O_8 (right) powder particles at the same magnification (2 300×).

UO2 powders with different properties and sinterability are shown in Figure 20. Variations in specific surface area will not show in SEM images since it is mostly dependent on porosity. Notice also that the sample size for measuring the mean particle size Dv50 is a few grams of powder, and in the image only a handful of particles are shown. The difficulty lies in a representative sample. However, the SEM image library can be used in the future in investigations of odd powders with deviating behavior.

U_3O_8-addition according to evaluation (sinterability)	2.0%	3.8%	12.1%
Specific surface area [m^2/g]	5.30	5.38	5.39
Dv50 [µm]	23.30	20.50	21.80

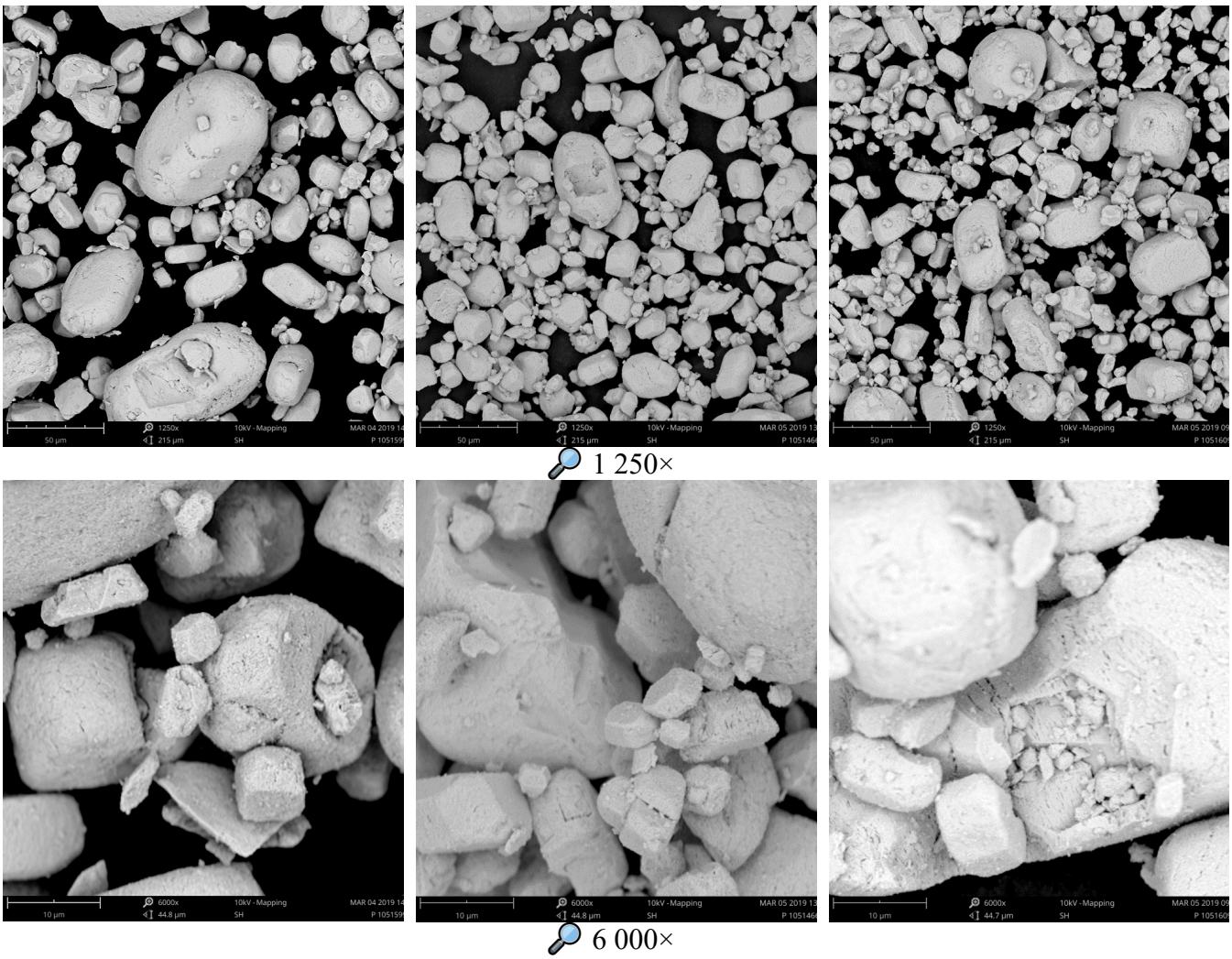

Figure 20. SEM images of 3 different UO_2 powders and some of their properties. From left to right the powders are determined to have low, medium, high sinterability as per the calculated U_3O_8 powder addition . The samples in the images are not blended with U_3O_8 powder.

4 Conclusions

- The determination of suitable U_3O_8 powder addition can be improved by taking the diameter shrinkage into account. Grinding waste can be minimized by adapting the pressure according to the diameter shrinkage. This procedure has been implemented in the production.
- The sinterability phenomenon is better predicted by a combination of parameters.
- Sintered density is not shown to be dependent on U_3O_8 powder batch, however shrinkage is in one case.
- Mixed powders do not necessarily behave as the average of their constituent virgin powders. Properties examined are sintered density, specific surface area and average particle size Dv50. Powder blends A2 (active/active) and G2 (inactive/inactive) behave similarly, and both decrease the specific surface area and increase sinterability compared to the virgin powders. This unexpectedly defies the theoretical outcome.
- The rate of oxidation is equal for active and inactive UO_2 powders under equal specific surface area/solution volume ratio where the powders had different specific surface area.
- SEM image library of various powders started, is to be used in future investigations as reference.

5 Future work

- Determination of U_3O_8 powder addition: formulate as an optimization problem to:
  - determine optimal manufacturing parameters given input data
  - minimize deviation from nominal values for e.g. pressure, grinding margin
  - include either U_3O_8 powder addition, or production yield in the objective function.
- Take a machine learning approach to data analysis using powder and pellet characteristics to train a neural network to predict optimal outcomes.
- Conduct further experiments on chemical activity.
  - More variations of UO_2 powders, including blended powders with U_3O_8 powder addition,
  - Especially contradicting powders:
    - UO_2 with high specific surface area, but inactive (low sinterability)
    - UO_2 with low specific surface area, but active (high sinterability).

6 References

[1] World Nuclear Association. "*Heat Values of Various Fuels*." World-Nuclear.org, 2018, www.world-nuclear.org/information-library/facts-and-figures/heat-values-of-various-fuels.aspx.

[2] R.K. Pachauri and L.A. Meyer (eds.). *"Climate Change 2014: Synthesis Report. Contribution of Working Groups I, II and III to the Fifth Assessment Report of the Intergovernmental Panel on Climate Change."* IPCC, Geneva, Switzerland, 2014, pp.151

[3] International Atomic Energy Agency (IAEA). "*PRIS - Nuclear Share of Electricity Generation in 2018*." IAEA.org, 2018, pris.iaea.org/PRIS/WorldStatistics/NuclearShareofElectricityGeneration.aspx.

[4] Strålsäkerhetsmyndigheten. "Så Fungerar Ett Kärnkraftverk." *Strålsäkerhetsmyndigheten*, 27 May 2019, www.stralsakerhetsmyndigheten.se/omraden/karnkraft/sa-fungerar-ett-karnkraftverk/.

[5] Westinghouse. "Nuclear Energy." *Westinghouse Nuclear*, 2014, www.westinghousenuclear.com/.

[6] Runfors, Ulf. "*Influence of Power Characteristics on Process and Product Parameters in* UO_2 *Pelletization*." OSTI.gov, 1971, www.osti.gov/biblio/4707352-influence-power-characteristics-process-product-parameters-uo-sub-pelletization.

[7] Glodeanu, F., et al. "*Correlation between* UO_2 *Powder and Pellet Quality in PHWR Fuel Manufacturing*." Journal of Nuclear Materials, vol. 153, Apr. 1988, pp. 156–159, www.sciencedirect.com/science/article/pii/0022311588902073, 10.1016/0022-3115(88)90207-3.

[8] C Ganguly and R.N. Jayaraj. "*Characterisation and Quality Control of Nuclear Fuels*. International Conference on Characterisation and Quality Control of Nuclear Fuels 2002, Allied Publishers, 2004.

[9] Yang, Jae Ho, et al. "*Recycling Process for Sinter-Active U3O8Powders*." Journal of Nuclear Science and Technology, vol. 47, no. 6, June 2010, pp. 538–541, 10.1080/18811248.2010.9711976.

[10] Hälldahl, Lars. "*Studies of Reactions Occurring in the AUC Process: From UF6 to Sintered* UO_2 *Pellets*." Chemical Communications, 1985.

[11] OECD Nuclear Energy Agency. "*Reference Values for Nuclear Criticality Safety: Homogeneous and Uniform* UO_2*, 'UNH',* PUO_2 *and 'PuNH', Moderated and Reflected by H2O*." OECD Nuclear Energy Agency, 2006.

[12] Lousada, Cláudio M., et al. "*Catalytic Decomposition of Hydrogen Peroxide on Transition Metal and Lanthanide Oxides*." Journal of Molecular Catalysis A: Chemical, vol. 379, Nov. 2013, pp. 178–184, 10.1016/j.molcata.2013.08.017.

[13] Hochanadel, C. J. "*Effects of Cobalt γ-Radiation on Water and Aqueous Solutions*." The Journal of Physical Chemistry, vol. 56, no. 5, May 1952, pp. 587–594, 10.1021/j150497a008.

[14] Ghormley, J. A., and A. C. Stewart. "*Effects of γ-Radiation on Ice*." Journal of the American Chemical Society, vol. 78, no. 13, July 1956, pp. 2934–2939, 10.1021/ja01594a004.